ORIGINAL ARTICLE

CrossMark

Iterative simulations to estimate the elastic properties from a series of MRI images followed by MRI-US validation

Francesco Visentin[1,2] (ID) · **Vincent Groenhuis[3]** · **Bogdan Maris[2]** · **Diego Dall'Alba[2]** · **Françoise Siepel[3]** · **Stefano Stramigioli[3]** · **Paolo Fiorini[2]**

Abstract

The modeling of breast deformations is of interest in medical applications such as image-guided biopsy, or image registration for diagnostic purposes. In order to have such information, it is needed to extract the mechanical properties of the tissues. In this work, we propose an iterative technique based on finite element analysis that estimates the elastic modulus of realistic breast phantoms, starting from MRI images acquired in different positions (prone and supine), when deformed only by the gravity force. We validated the method using both a single-modality evaluation in which we simulated the effect of the gravity force to generate four different configurations (prone, supine, lateral, and vertical) and a multi-modality evaluation in which we simulated a series of changes in orientation (prone to supine). Validation is performed, respectively, on surface points and lesions using as ground-truth data from MRI images, and on target lesions inside the breast phantom compared with the actual target segmented from the US image. The use of pre-operative images is limited at the moment to diagnostic purposes. By using our method we can compute patient-specific mechanical properties that allow compensating deformations.

Keywords Magnetic resonance imaging · Elastic properties · Breast · Image alignment · Deformable models

1 Introduction

Imaging techniques are important for screening and diagnosis to determine the location of a tumor in breast cancer. To end up with the same location during the common workflow, the effect of deformations should be taken into account for accurate corrections of the static situation.

Breast cancer diagnosis and surgery are based on different image acquisition modalities ranging from mammography (x-ray), US, and MRI. The method with the highest sensitivity is MRI [1]. The biopsy procedure or the surgery could benefit from the transfer of information from the pre-operative imaging into the operating room. In fact, the position of the patient varies from the prone, during the MRI scanning, to the supine position which is required for the breast biopsy or surgery. During US scanning and US-guided biopsy, the patient is reclined on her back and additional compression is induced by the US probe. To end up with the same location during the workflow (e.g., diagnostic imaging, biopsy procedures), the effect of deformations should be taken into account for accurate corrections of the static situation.

Three-dimensional models of the breast can be reconstructed using MRI volumetric data. To properly model all the deformations, it is important to estimate the elastic properties of the tissues under examination. Mechanical properties of the breast tissue have been measured on ex vivo samples [2, 3]. Techniques to measure the elastic properties of in vivo breast tissue are based on sono-elastography, magnetic resonance elastography, shear wave elasticity imaging, and mechanical imaging [4–6]. In vivo measurements are limited due to the small deformation experiments, while the mechanical properties of ex vivo samples are different from in vivo tissues due to the fixation of tissue samples and other effects. It is also generally known that the mechanical properties of the breast tissue vary across

---

F. Visentin and V. Groenhuis contributed equally to the paper.

✉ Francesco Visentin
francesco.visentin@iit.it

1 Istituto Italiano di Tecnologia, Center for Micro-BioRobotics, Viale Rinaldo Piaggio 34, 56025 Pontedera, Pisa, Italy

2 Universitá di Verona, Strada le Grazie 15, 37134 Verona, Italy

3 University of Twente, Drienerlolaan 5, 7522NB Enschede, The Netherlands

the population and over time for each person, meaning that patient-specific models should be considered to achieve an accurate estimation.

Most of the studies involve the use of FE models to solve for the large deformations of the breast [7, 8]. A patient-specific biomechanical model that provides an initial deformation of the breast between prone and supine MRI images was proposed in [9]. A zero-gravity reference state for both prone and supine configurations was estimated. The authors performed a comparison of three methods to obtain the patient-specific unloaded configuration [10].

Most of the times, the biomechanical methods serve for the initialization of intensity-based image registration techniques [11, 12]. The sliding motion of the breast on the chest wall was observed [13], but usually, a fixed muscle surface is applied during the FE simulations [12, 14, 15].

Another approach to model the breast deformation is based on mass-spring models (MSMs). The MSMs are easier to implement but their main drawback is their intrinsic non-realistic tissue mechanics representation, due to the local distribution of the mechanical parameters characterizing the model. A 3D female breast deformation model based on MRI data and MSMs iterative deformation was implemented in [16]. Compared to FE-based methods, MSMs allows for a realistic representation of tissue resection and can be easily parallelized [17]. In FE applications, removing a mesh element requires recalculation of the mesh constraints and re-meshing of the whole structure, but in the applications that do not take into account the resection, the FE approach is preferred.

In this work, we used the FE framework to compute the displacement induced by the gravity force on the breast tissue by comparing two MRI acquisition: the prone and the supine. The approach is motivated by the fact that in these two configurations the gravity force lays on the same line, but has opposite direction. Using such simplification, we are able to derive an "at rest" configuration, where no forces are acting. This can be used to generate any configuration of the breast (e.g., lateral, vertical) by properly setting the direction of the gravity force and the applied external forces. The method, validated on different anatomical phantoms using MRI and US data, can be used to predict the location of lesions and use such information in pre-operative planning of biopsy when, to limit patients' discomfort, it is crucial to perform the exam with high precision.

The paper is structured as follows: in Section 2, we will introduce the mathematical background of the method, the fabrication process of the phantoms, the protocol used to acquire MRI data, and the processing applied to the DICOM images. Section 3 presents the experimental setup, and it will introduce the FE framework used. Results and their discussions are presented in Section 4, followed by Section 5 for conclusions and future works.

2 Materials and methods

2.1 Global motion of the breast

The deformation of the breast is due to the body movement, therefore before applying a deformation method, a rigid motion should be recovered. The rigid motion is completely described by 6 degrees of freedom, of which 3 for rotation and 3 for translation. A more general class of transformations are the affine transformations, which have six additional degrees of freedom, describing scaling and shearing. In the three-dimensional space, an affine transformation can be written as:

$$\begin{bmatrix} \mathbf{y} \\ 1 \end{bmatrix} = \begin{bmatrix} A & \mathbf{b} \\ 0 & 1 \end{bmatrix} \begin{bmatrix} \mathbf{x} \\ 1 \end{bmatrix} \tag{1}$$

which is equivalent to the following:

$$\mathbf{y} = A\mathbf{x} + \mathbf{b}. \tag{2}$$

In these equations, $\mathbf{x}$, $\mathbf{y}$ are the input/output vectors, the matrix A encodes the rotation, shearing, and scaling transformations, while the column vector $\mathbf{b}$ is the translation.

Affine transformations can be directly applied in image registration or can be used as an initialization of more complex non-rigid registration. In [18], the authors showed that the affine registration is preferred over other more complex non-rigid transformation when registering x-ray mammography with MRI deformed by FE. Another study about affine transformation applied to mammography registration [19] reported an error of 8 mm computed as the average distance between the target lesions after the registration.

2.2 Elastic properties of isotropic materials

Almost any solid body, anchored at one end and pulled at the other with a force F, will react like a spring. Real springs, like ideal ones, are elastic elements obeying Hooke's law ($\mathbf{F} = k\mathbf{x}$) that states the proportionality (k) between the applied force ($\mathbf{F}$) and the change of length of the spring ($\mathbf{x}$). In general, it is more important to consider the average normal stress along the direction of the force than the force modulus to extend the length of a spring. By combining the ratio between the applied force and the area of the spring with the relative longitudinal extension, it is possible to obtain a quantity that represents the behavior of the material when stretched in one direction:

$$E = \frac{\mathbf{F}/A}{\mathbf{x}/L} = k\frac{L}{A}, \tag{3}$$

where $\mathbf{F}$ is the applied force, A the area of the string, L its length, and k the proportionality stated by the Hooke's

law. This ratio, called the *Young's modulus*, is constant everywhere along the string and it represents a measure of in-stretchability. The larger it is, the harder is to stretch the material.

Another quantity used to model the behavior of an elastic material is the *Poisson's ratio*. This measures the ratio between compression (stress) along the transverse direction (u_{yy}) to the extension (u_{xx}). The material constant is dimensionless, cannot exceed 0.5, and it is described by the following equation:

$$\nu = -\frac{u_{yy}}{u_{xx}}. \tag{4}$$

If the material taken into consideration is isotropic (deform similarly along all directions), to express Hooke's law such that takes the same form in all coordinate systems, it is needed to derive a linear relationship between the complete stress tensor, σ_{ij}, and the complete strain tensor, u_{kk}. The most general linear relationship between strain and stress [20] is defined by

$$\sigma_{ij} = 2\mu u_{ij} + \lambda \delta_{ij} \Sigma_k u_{kk}. \tag{5}$$

where λ and μ are material constants, called elastic moduli or Lamé coefficients, δ_{ij} is the Kronecher delta, $\Sigma_k u_{kk}$ the trace, and ij indicate the tensor along any arbitrary direction. It is possible to express the Young's modulus and the Poisson's ratio as the relationship of λ and μ as follows:

$$E = \frac{\mu(3\lambda + 2\mu)}{\lambda + \mu}, \quad \nu = \frac{\lambda}{2(\lambda + \mu)}. \tag{6}$$

Using this pair of elastic moduli, it is possible to fully describe the elastic properties of any homogeneous and isotropic material.

2.3 Estimation of the elastic modulus from volumetric data

In this work, for simplicity, we assumed the breast tissues as a unique isotropic homogeneous material subjected only to the gravity force. Such material, placed on a horizontal surface, has the same properties, everywhere along the horizontal plane, as a fluid. In Earth coordinate system, gravity is given by $\mathbf{g} = (0, 0, -g_0)$, therefore, we expect a uniform vertical displacement, which only depends on the z−coordinate: $\mathbf{u} = (0, 0, u_z(z))$. On the top, $z = h$, h is the total height of the model, the elastic material is left free to move without any external forces acting on it. At the bottom, $z = 0$, we place a rigid planar constraint, that allows the only displacement in the horizontal directions (x and y). The only strain that does not vanish is the one related to the z−direction, u_{zz}, and expressing it using Eq. 5 gives

$$\sigma_{xx} = \sigma_{yy} = \lambda u_{zz}, \quad \sigma_{zz} = (\lambda + 2\mu)u_{zz}. \tag{7}$$

Using the boundary condition $\sigma_{zz} = 0$ at $z = h$ to the simplified Cauchy's equilibrium equation, and integrating the strain with the boundary condition it brings to

$$\sigma_{zz} = -\rho_o g_0 (h - z). \tag{8}$$

This also expresses the vertical pressure along the body. The strain,

$$u_{zz} = \nabla_z u_z = -\frac{\rho_0 g_0}{\lambda + 2\mu}(h - z), \tag{9}$$

is negative, due to the choice of the reference frame, and it corresponds to a compression. Integrating the strain with the boundary condition $u_z = 0$ for $z = 0$, we obtain

$$u_{zz} = -\frac{h^2 - (h - z)^2}{2D}, \tag{10}$$

where $D = \frac{\lambda + 2\mu}{\rho_0 g_0}$ is the characteristic length scale for major deformation.

Knowing the total displacement, D, and assuming constant the value of the *Poisson's ratio*, it is possible to derive the value of the *Young's modulus*. For the case of the breast tissue, it is not possible to obtain the value of the displacement with respect to an "at rest" situation, instead, it is possible to compute it with respect to another configuration.

2.4 Phantom fabrication

Four phantoms were constructed (Fig. 1, left) for this study. Each phantom, named with letters from E to H, consists of a rigid base, stiff superficial tissue, soft deep tissue, and three to four lesions. The base is a 3D printed structure made of polylactide (PLA) and houses three vaseline markers with a diameter of 10 mm. The markers, or fiducials, are used for rigid alignment. The base also mimics the rib cage, providing a rigid attachment to the flexible phantom, and can be attached to a frame that serves to place the phantom in the four different positions (Fig. 2). The superficial and deep tissues and lesions are made of polyvinyl chloride (PVC) with a plasticizer, mixed in different ratios in order to obtain a relatively high stiffness for superficial tissue and lesions, and low stiffness for deep tissue.

The fabrication was divided into two main steps. First, the superficial tissue was molded in the desired shape using the inner and outer molds (Fig. 1, right). Next, the inner mold was removed and the empty space was filled with soft PVC. Inside this, three to four stiff pieces of PVC have been placed to simulate the presence of lesions inside the breast tissue. Finally, the base was placed on top of the deep tissue's PVC and covered with stiff PVC. The external shapes of the four phantoms are identical, the
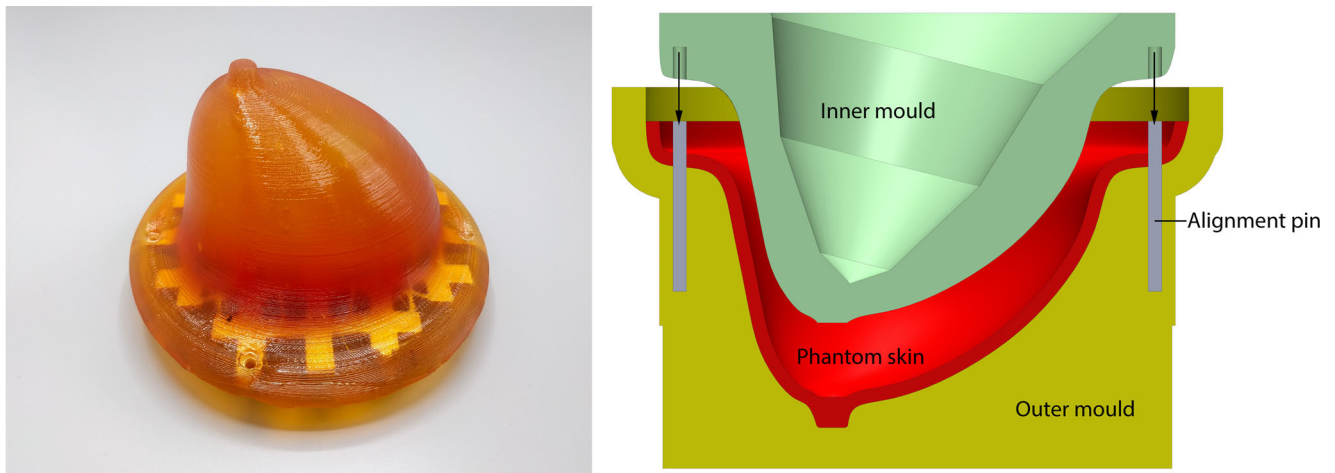
Fig. 1 Left: one PVC breast phantom. Right: a pair of molds for manufacturing superficial and deep tissues
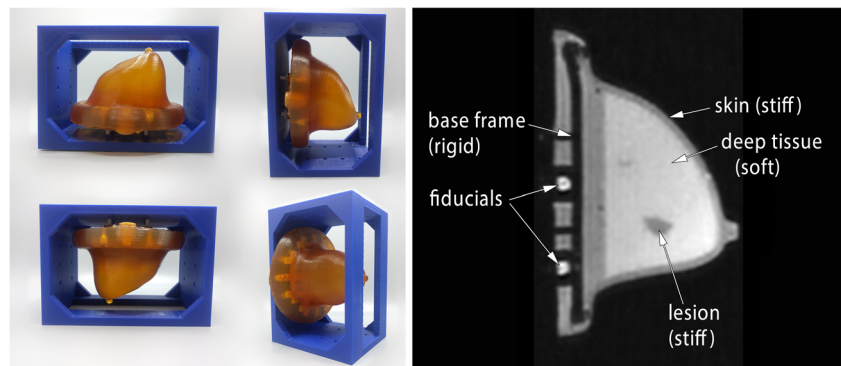
only differences are in the stiffness of deep tissue and the placement of lesions.

2.5 MRI scanning

Each of the four phantoms was scanned in a 0.25 T Esaote G-scan Brio MRI scanner. The chosen scanning protocol is 3D Hyce, which is a 3D balanced gradient echo sequence. This sequence combines good contrast between the different materials, in particular, PVC of varying stiffness. The scan time is 2:34 min, excluding pre-scan calibration (1:25) and post-processing (1:30). The acquisition voxel size is $1.5 \times 1.8 \times 2.0$ mm. The resulting scans have good signal-to-noise ratio, as required for effective segmentation.

Each phantom was scanned in four orientations, as shown in Fig. 2. Figure 2, right, shows one sagittal slice of the phantom in the vertical position, pointing out the different components of the phantom. It can be observed that the scan has different signal intensities for the superficial tissue (skin), deep tissue, lesions, base frame, and fiducials and that the image is sufficiently smooth and uniform to allow direct segmentation by thresholding.

2.6 Data pre-processing

The first step is the identification and segmentation of the base markers (Fig. 2, right). These were used to align the prone, vertical, and lateral models to the supine model by calculating the rigid transformation that maps the three fiducials such that the error, defined as the root-mean-square of the fiducial distances, is minimal. This error was found to be, on average, in the range of 0.2–0.3 mm for all phantoms in all orientations. Figure 3 shows two configurations of a phantom, overlaid on each other, after segmentation and rigid registration. In both cases, a displacement of the tip resulting from the gravity field (oriented downwards in both figures) can be observed.

After the alignment of the MRI images, we segmented separately the breast phantom, and the lesions by using an automatic algorithm based on region growing and threshold. Smoothing and decimation processes were employed to improve the quality of the surface reconstruction. The 3D volumetric models were generated in a total of ten different levels of detail, for FE analysis. These different mesh resolutions were constructed by first downscaling the
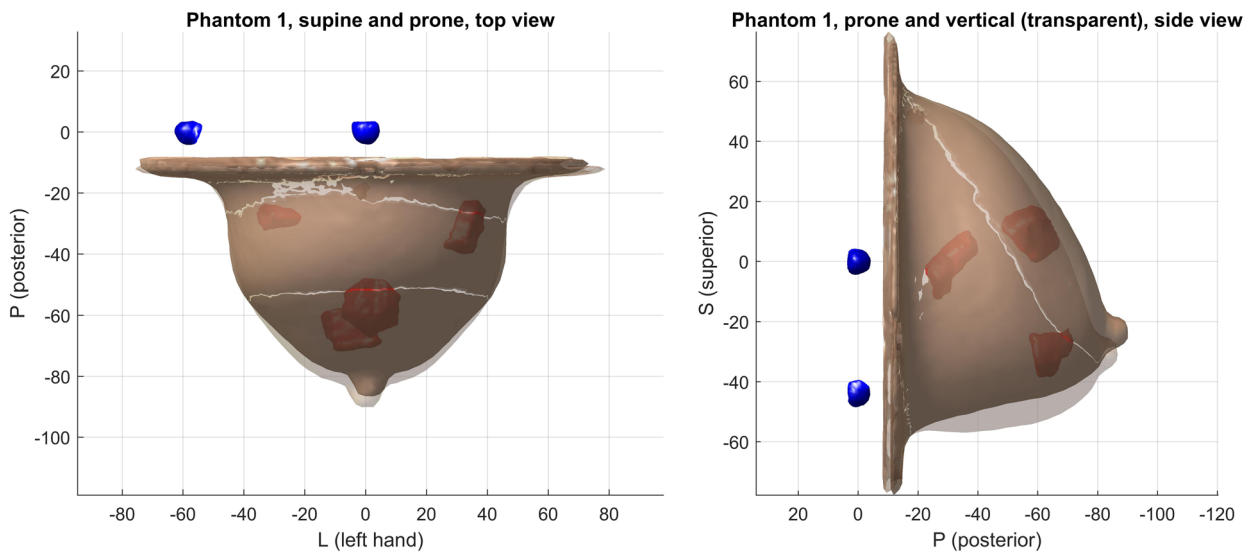
Fig. 2 Left: the four breast phantom orientations in scanning. Clockwise, from top-left: supine, vertical, lateral, and prone orientations. Right: example of sagittal MRI slice

Fig. 3 Left: phantom in prone and supine configuration, superimposed after rigid registration based on markers visible on the top. Right. phantom in prone and vertical position, superimposed after rigid registration based on the markers visible on the left side. The gravity acts in the vertical direction

original DICOM data by a certain factor (between 0.05 and 0.40 in ten steps), followed by segmentation of the downscaled DICOM data. The same process has been also applied to each of the lesions presents in the phantoms. The entire workflow is depicted in Fig. 4.

3 Experimental setup

To prove the capability and the adaptability of our approach, we performed a series of analyses using different phantoms. We validated the method by comparing the FE simulations results with a ground truth acquired using an MRI scanner (single-modality validation), or in combination with US images (multi-modality validation).

We first estimated the elastic parameter of four phantoms developed as previously described. Each phantom has been placed in the MRI scanner in four different configurations: prone, supine, lateral, and vertical (Fig. 2, left). The acquired data were then pre-processed to align them rigidly

with respect to a common reference system by using markers visible in the MRI data (Fig. 3).

The external surface of the breast phantom and the surface of the internal lesions were merged into one single surface mesh used in the FE analysis. A 3D Delaunay tetrahedralization was then applied to create a volume mesh. The resulting mesh is a homogeneous volume with internal empty structures representing the lesions. For this reason, the breast tissue was modeled as an isotropic elastic material, while the lesions were modeled as incompressible semi-rigid material. An FE analysis software (FEBio [21]) was then used to simulate the biomechanical behavior of the breast phantom, and to estimate the specific elastic parameter of each breast phantom.

We based the estimation of the Young's modulus E of the isotropic material on the change between two configurations: supine and prone. After an initial guess of E, we iteratively compare the results of the simulations with the target mesh. The matching error, either computed on the whole mesh or on a subset, is used with the Newton's
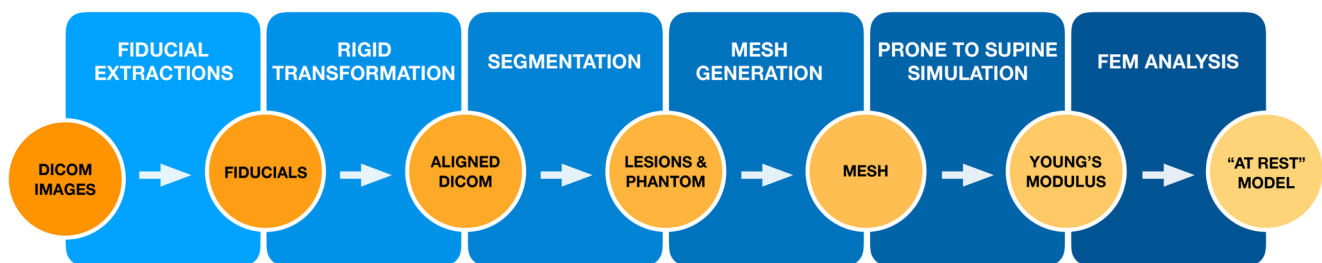

Fig. 4 Workflow of the proposed method. In the figure, boxes represent processing steps, while circles are used to identify output of the single steps

method to estimate a new value for the parameter. The process stops when a target error is reached, i.e., the change of the parameter is lower than a pre-defined threshold, or if a fixed number of steps has been reached. To ensure correctness in the estimation, we performed both the change of configuration from prone to supine and vice versa. At the end of the process, the square harmonic mean $((4 * \sqrt{A * B}/(\sqrt{A} + \sqrt{B}))^2)$ of the returned values is used as a final value. With the estimated Young's modulus, we generate an "at rest" mesh model, where no forces are acting. This mesh can be used to simulate other configurations by changing the direction of the gravity force.

3.1 Single-modality setup

We validated our approach by comparing the matching error between each of the acquired configurations (prone, supine, vertical, and lateral) with the simulated configurations. We estimated both the matching error with respect to the superficial nodes of the mesh, and with respect to the centroids of each lesion. Since there is no direct correspondence between the nodes of the different meshes, we took the closest point to point distance, as in [22], to minimize the difference between two sets of nodes. In this study, each phantom extends horizontally (back to front) along the positive direction of the y-axis, and vertically (bottom to top) along the positive direction of the z-axis. With this alignment, to generate the prone configuration it is needed to apply the gravity force of 9.8 N along the y-axis, while to generate the supine one a -9.8 N force along the same axis. The vertical configuration, instead, is obtained by applying -9.8 N along the z-axis, and to generate the lateral configuration it is needed a force of -9.8 N along the x-axis. Figure 5 shows the directions of the x-,y-, and z-axes.

3.2 Multi-modality setup

The standard US breast diagnosis setup setup involves the identification of the target (lesion) in pre-operative, high-resolution MRI acquired in the prone position and the tissue sampling with the patient on semi-supine position. To test the adaptability of the method in a realistic clinical setting,

we compared the results obtained with FE simulations with measurements acquired from MRI data in combination with US. The aim of this second analysis is to evaluate the performance of the proposed FE simulation methods in compensating for breast deformation introduced by US scanning. In this study, we only consider the deformations induced by the gravity force when scanning the phantom in different positions between supine and prone orientations. Since the phantoms used in the previous section are not compatible with US acquisitions, we employed a multi-modality breast phantom CIRS 0731 (CIRS Inc.) that accurately mimics heterogeneous breast tissue appearance under different imaging modalities such as US, MRI, mammography, and CT.

To limit the motions of the phantom, and to facilitate US acquisitions, we rigidly attached the phantom to a rotating table to mimic the different scanning positions. We considered angles from 0 to 180°, corresponding respectively to supine and prone scanning position, measured with respect to the floor plane. Between the two extremes, we only considered the deformations induced by the gravity force when scanning the phantom in different positions between supine and prone orientations. A total of 13 scanning position each of them acquired with steps of 15°. In each of the scanning, the position of the table has been locked and the US acquisition has been performed using a freehand US system (FUS). The FUS setup (Fig. 6) is based on a Sonix MDP US machine (Ultrasonix, Richmont, Canada) and a Micron Tracker H×40 tracking system (Claron Technology, Toronto, Canada). We performed the calibration with a linear probe (model L14-5/38) with an acquisition frequency of 10 MHz and a depth setting of 60 mm, using hardware and software components provided by the PLUS toolkit [23]. More detailed description of the experimental setup, including coordinate reference systems relationship, is available in [24]. We fixed a coordinate reference system to the phantoms so that the three-dimensional information reconstructed from the FUS system is independent of the table rotation angle. Using markers visible on the phantoms and the tracking system, all the acquisitions are aligned rigidly in a common reference system. Through FUS we identify the central point of the lesions inside the

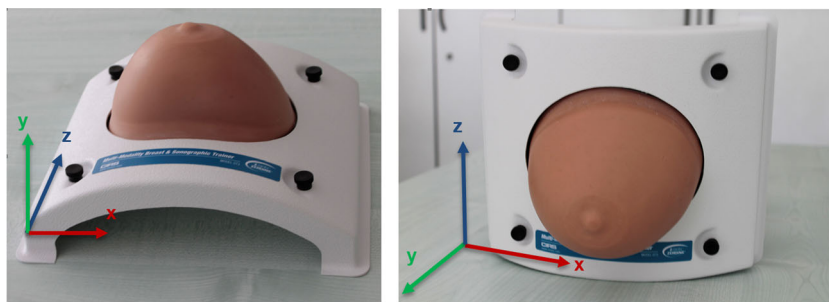**Fig. 5** The multi-modality phantom and the xyz reference system

Fig. 6 The multi-modality setup uses an optical tracker and markers that define a reference system attached to the breast phantom. The US probe is tracked as well

phantom which are then mapped in the tracking reference system.

To replicate the same configuration also in the FE framework, we scanned the phantom using the protocol introduced earlier and processed the acquisitions to obtain the volume meshes. These have been used to estimate the phantom's elastic property and to validate the value following the same steps used for the other phantoms. From these initial analysis, we synthesized a mesh in which the breast was not subjected to any gravity force (i.e., the "at rest" configuration) that was placed in the same reference system as the one used in FUS acquisitions. In this configuration, to replicate the change of orientation of the table, we applied a series of transformation matrices to the vector representing the gravity force. For every step (15°), we extracted the centroids of each lesion and compute the distance from the same centroids acquired in the US data. To evaluate the effects due to the FE analysis error, we also computed the distance between a non-rotated mesh placed in the same reference system.

4 Results and discussions

All the computations, both registration, and FE analysis, have been performed on a 2.6 Ghz i7 machine with 16 GB of RAM. The generated meshes contain around 34000 nodes forming 123000 4-node tetrahedron elements. From the computational point of view, the time required for each simulation differs according to the stiffness of the material. Stiffer materials take shorter computation time ($\sim$2 s), while softer materials require a longer time ($\sim$20 s). In total, the parameter estimation required around 2–5 min. We need to consider that current implementation is not optimized, therefore reduction of estimation time is possible by implementing the FE solution using parallel hardware (i.e., GPU). Therefore, we expect a final estimation time under 1 min, compatible with clinical practice. Results are grouped according to the experimental setup presented earlier.

4.1 Single-modality validation

Table 1 presents the estimated values for the Young's modulus for each of the tested phantom. The mean value of the supine-to-prone (SP) and prone-to-supine (PS) has been computed as the square harmonic mean and used in later validations. As the results suggest, there is a consistency in the value of the elastic parameter computed for both directions. The fact that the values obtained in the two configurations are not identical relies on the presence of stiff masses within the phantoms, causing their behavior to displace from the ideal isotropic condition we are considering. Despite this, it is possible to observe an overall consistency in the value of the elastic parameter computed for the two directions, meaning that the isotropic approximation holds in this setup (since stiff masses are small and inserted in a homogeneous material). However, when clinical data will be used, an isotropic assumption may not stand and a different material might be used.

Results on prone to supine matching are shown in Fig. 7. In the figure, blue color represents small errors,

Table 1 Elasticity computed using the iterative method presented in the paper

	SP	PS	Mean
E	5397.14	6129.98	5746.08
F	3950.24	4197.28	4070.95
G	5342.15	5695.93	5514.79
H	7839.15	8314.50	8071.58

SP stands for supine-to-prone, while PS stands for prone-to-supine. The value expressed by Mean is the square harmonic mean between the SP and PS values. All values are expressed in kPa
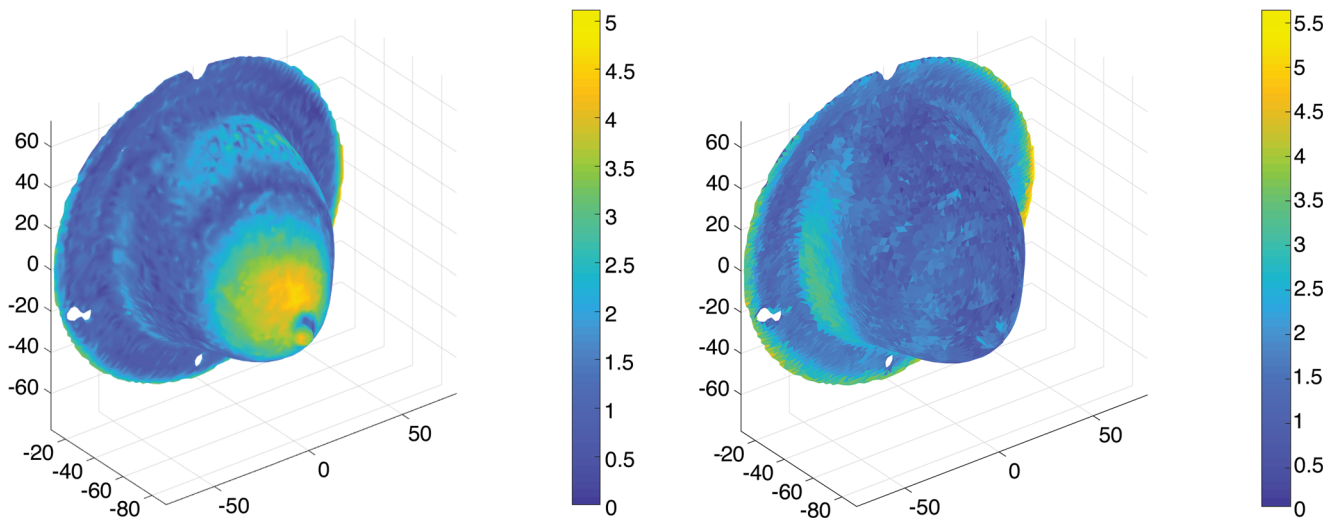
Fig. 7 Prone-supine model matching between the segmented surfaces. (left) The initial error just after registration. (right) The final error after the gravity-only induced deformation. For both cases, a color bar representing the magnitude of the error is shown. The value expressed in the color bars has to be intended in mm

while yellow represents larger errors. In the picture, the region subjected to a higher change—i.e., where the error is reduced by the applied deformation—is the one closed to the front part of the phantom. This phenomenon is expected since the back part of the phantoms is fixed to an external rigid structure that constrained its deformation. The front part, instead, is free to move following the direction of the applied force. Thanks to this result, we could reduce the number of points over which we compute the matching errors in the validation phase. In fact, instead of using the whole cloud of points, we could limit the comparison only to the subset that was within the 20–30% of the total distance from the front part of the mesh. This can reduce the computation time while preserving accuracy in the computation of the error. Table 2 presents the validation errors computed using such subset of points for all the considered cases (i.e., supine, prone, lateral, and vertical).

Each error is computed with respect to the initial non-deformed mesh, and after the application of the gravity force along the proper direction. As reported in the table, there is a common trend in reduction of the global error. Despite this, the errors are not reduced to zero. This can be explained by the fact that there is not a direct matching between the nodes of the different meshes, and by the fact that the phantoms are not always perfectly aligned with the real direction of the aplied force.

We also measure the matching error between the centroids of the lesions (Table 3). When lesions are taken into account, results on centroid displacement errors are smaller with respect to global displacement error, this is due to the fact that the lesions were made of a stiffer material than the rest of the phantom. As a consequence, the displacement of the structure is smaller. In both tables, it is possible to notice a smaller error in the prone configuration. This is due to

Table 2 Initial and final errors between the reference model and each of the views before applying any further deformation

|	Supine		Prone		Lateral		Vertical	
E	3.672	2.499	2.579	1.033	7.337	2.722	7.172	2.311
F	4.630	3.813	3.227	1.078	9.395	3.810	8.292	3.500
G	3.972	2.834	3.075	1.497	6.902	4.259	7.666	2.456
H	3.500	2.908	2.063	0.791	5.943	1.886	7.831	3.069

The error has been computed on a subset of points within 5% of a distance from the nipple area of the breast. If a wider area is considered, no significant changes in reported values are noticeable. All the values are expressed in mm. For each case, the first column is the mean error before force application, and the second one is the mean error after force application

Table 3 Mean error on lesion matching per view and per phantom

	Supine		Prone		Lateral		Vertical	
E	1.660	1.136	1.084	0.066	4.156	1.185	4.271	0.869
F	1.921	1.385	1.775	0.061	6.163	2.195	7.080	0.888
G	0.952	0.929	0.914	0.041	2.670	1.524	3.456	0.770
H	1.777	0.913	1.282	0.063	4.386	1.189	5.705	1.142

The errors (in mm) are computed with respect to the position centroid of each lesions before (first column) and after (second column) applying the gravity-only-induced deformation. Phantom H has only 3 lesions instead of 4 as in the other cases. The prone case is the one that shows smaller error since the reference model has been constructed from the prone one. As a consequence, the error between the matching points is smaller

Fig. 8 Errors for US-FEM matching. (top) Errors computed with respect to a rigid model that rotates but it is not affected by any force. (bottom) Errors computed with respect to the results of FE analysis. As the image suggests, the use of FE analysis allows to reduce the displacement errors but does not cope with the applied force from the US probe
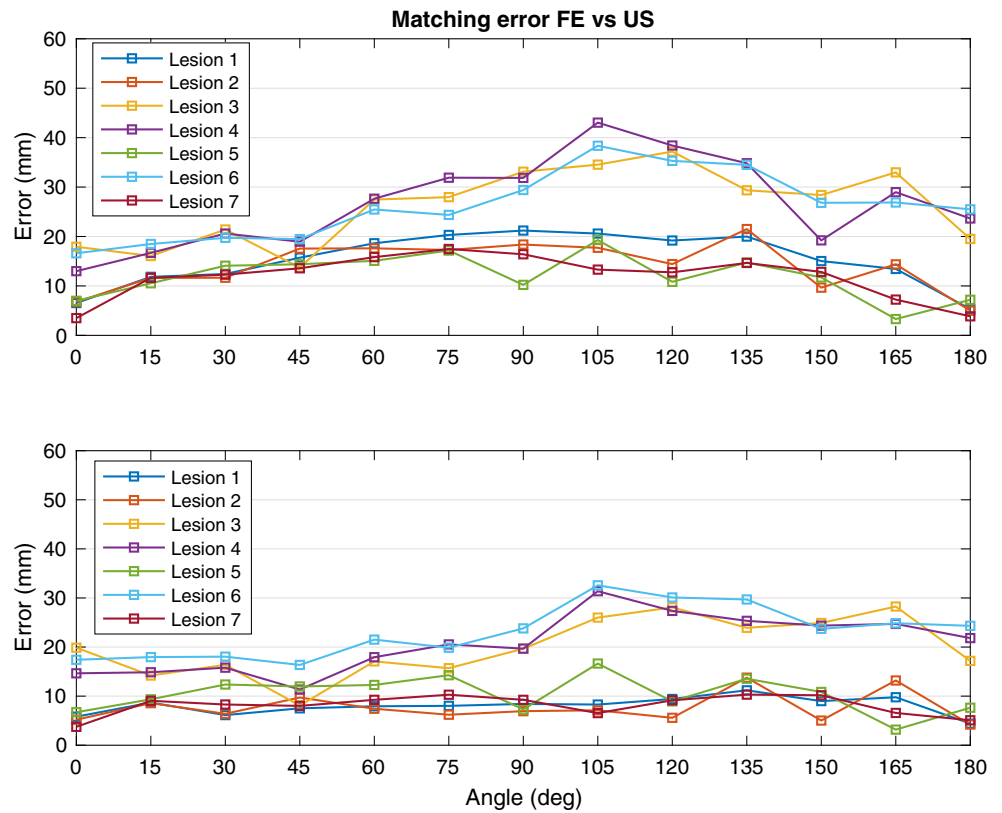

the fact that to generate the initial mesh (the one in-between the prone and the supine configuration), we used the points of the prone model. As a consequence, the match between the nodes is more precise and the errors are reduced.

4.2 Multi-modality validation

The elastic properties of the CIRS phantom are estimated and used to further validate the approach. The final value for

Fig. 9 Mean errors for US-FEM matching after removing an initial offset. (left) Results computed with respect to a fixed mesh that only rotate according to the prescribed motion. (right) Results obtained by FE analysis. In both cases, the first displacement error has bee used as a reference to compensate the force applied by the US probe during the FUS acquisitions
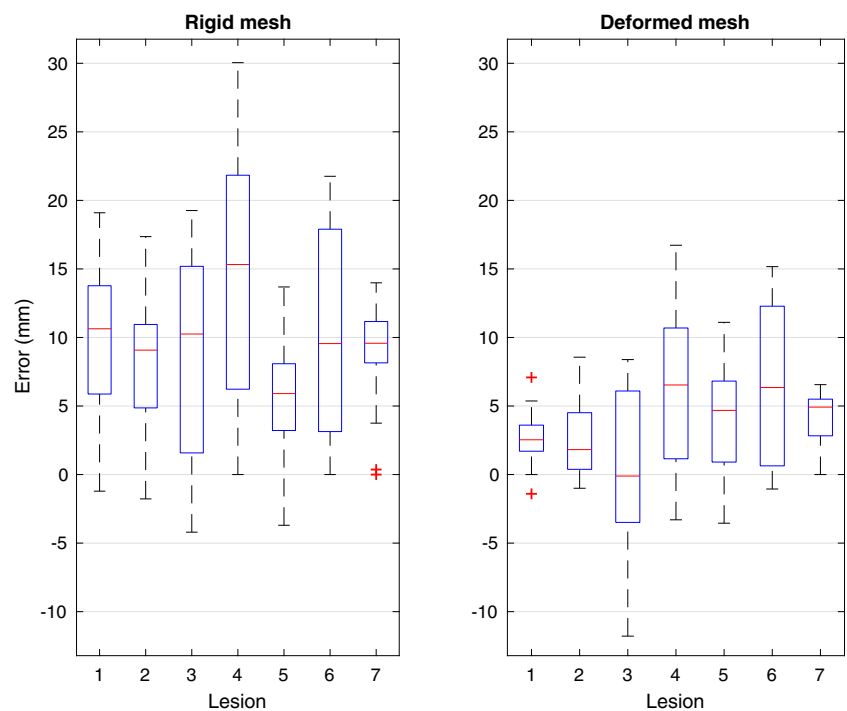
its Young's modulus is 2.85 kPa, which matches the control set points with an error of 0.65 mm. Differently from the previous case, we do not measure the superficial matching errors, instead, we only focus on the errors between the centroids of the lesions within the phantom. Figure 8 shows the matching errors of a non-deformed mesh, and the one obtained by the FE analyses with respect to the US data. As the image suggests, by simply rotating the model and not applying any body load, it is not possible to correctly follow the displacement of the lesions due to applied force. On the contrary, by applying a body load to the model it is possible to better approximate the position of the lesion centroids during the change from prone to the supine configuration. However, the simple application of the gravity force to the model is not sufficient and some errors still remain. This is due to the fact that we do not currently model the interaction between the US probe and the phantom.

In this study, we do not consider the compensation of the applied force during the FUS acquisition. However, if we assume it constant during the whole acquisition process (at every in-between step), we can use the initial displacement error as an approximation of the constant deformation applied by the US probe. Figure 9 shows the mean displacement value for each lesion present in the phantom both for the case of the fixed mesh and the one under the effect of the gravity force. As expected, the results relative to the rigid mesh still present higher matching error, while the errors computed with respect to the deformed mesh reduce their magnitude. Only two of the seven lesions still shows a mean error higher than 5 mm. These two lesions, 4 and 6 according to our enumeration, are placed, respectively, at the left and right side of the phantom, regions which we noticed being subjected to higher deformation than other portions of the same phantom. In addition, we noticed a high hysteresis of the material the phantom is made of. This, together with the non-uniform applied force might have influenced the obtained results.

5 Conclusions

In this work, we propose a framework to estimate the elastic properties of the breast tissue that can be used for diagnosis or for pre-operative planning. The technique is based on an iterative scheme in which two volumes (prone and supine) acquired from MRI images, were rigidly registered and then deformed by the action of the gravity force. We validated the method by using a series of realistic phantoms having different elastic properties. We placed each of them in an MRI scanner and acquired image data in four configurations: prone, supine, lateral, and vertical. These data were used as ground truth for FE analysis. In addition, we validated the method by combining MRI with US acquisitions of a commercially available, multi-modality phantom.

The results showed that the use of the proposed method allowed to reduce the global registration error between different configurations, even when these were synthetically created from FE analysis. Matching errors between the lesions were all within 2 mm and had an average overlap of 90%. This proved the correctness of the method in following the displacement of the phantom under the influence of the gravity force. When compared to other available methods, the one proposed in this paper did not only find the zero-gravity state ("at rest" model) to be used as a reference for non-rigid registration, but also allowed the estimation of synthetic views. Results obtained by comparing FE analysis with US data were less precise, but this was mainly due to the fact that in our model we did not cope with the displacement introduced by the interaction of the US probe with the phantom. In fact, as simplification, we assumed as constant the force applied from the US probe during the whole process and then removed an initial offset from all the measurements. Errors were still large, but promising as an initial step toward the estimation of patient-specific elastic properties—which is really important for the breast due to a high intra-subject variability of these properties—to be used in different medical applications.

Among these, a possible application is the one in which this technique is used as support in the common workflow for breast biopsy without adding significant modification. However, there are some limitations related to the use of the proposed approach. In fact, in a real scenario, the time constraints may not allow to perform the analysis of elasticity. In addition, target malignancy cells are usually scattered as multi spots making them difficult to track in real time. For these reasons, clinicians prefer to remove cells in different targets and in the proximity of a small volume. However, this work poses the basis for the development of technologies and controlling algorithms that can be used in biopsies guided by MRI or when a navigation system is used (e.g., an optical tracker or a biopsy robot) for the US guided biopsy. In fact, knowing the elastic properties, leads to the complete control over the deformation of the breast and allows the update of pre-operative data to match intra-operative data in a process called registration. The registration will be performed using a deformable model that employs the elastic modulus, as we have computed in this work. Including the registration in the clinical workflow offers potentially a significant improvement of the procedure and ensures a more precise targeting of early-stage lesions which are visible under MRI but not under US.

Future works will include clinical tests to adapt the method to the constraints imposed by the clinical context (e.g., time, distribution of the malignancy inside the breast tissue, reduced work space), and to validate the framework

on patient-specific characteristics. A multi-modality (e.g., MRI-US) registration test on patient data will be performed. The elastic properties computed through the presented method will be employed to compensate the interaction of the US probe with the tissue in contact. Single modality tests (e.g., MRI-MRI) will performed as well. Use of MRI visible markers that can support a coarse initial alignment and continuous tracking is also envisioned.

References

1. Sree SV, Ng EY-K, Acharya RU, Faust O (2011) Breast imaging: a survey. World J Clin Oncol 04(4):171–178
2. Samani A, Plewes D (2007) An inverse problem solution for measuring the elastic modulus of intact ex vivo breast tissue tumours. Phys Med Biol 52(5):1247
3. Gefen A, Dilmoney B (2007) Mechanics of the normal woman's breast. Technol Health Care 15(4):259–271
4. Parker KJ, Doyley MM, Rubens DJ (2010) Imaging the elastic properties of tissue: the 20 year perspective. Phys Med Biol 56(1):R1
5. Sarvazyan A, Hall TJ, Urban MW, Fatemi M, Aglyamov SR, Garra BS (2011) An overview of elastography-an emerging branch of medical imaging. Curr Med Imaging Rev 7(4):255–282
6. Doyley MM (2012) Model-based elastography: a survey of approaches to the inverse elasticity problem. Phys Med Biol 57(3):R35
7. Han L, Hipwell JH, Tanner C, Taylor Z, Mertzanidou T, Cardoso J, Ourselin S, Hawkes DJ (2011) Development of patient-specific biomechanical models for predicting large breast deformation. Phys Med Biol 57(2):455
8. Han L, Hipwell JH, Eiben B, Barratt D, Modat M, Ourselin S, Hawkes DJ (2014) A nonlinear biomechanical model based registration method for aligning prone and supine mr breast images. IEEE Trans Med Imaging 33(3):682–694
9. Eiben B, Han L, Hipwell J, Mertzanidou T, Kabus S, Bülow T, Lorenz C, Newstead GM, Abe H, Keshtgar M (2013) Biomechanically guided prone-to-supine image registration of breast mri using an estimated reference state. In: 2013 IEEE 10th international symposium on biomedical imaging (ISBI). IEEE, pp 214–217
10. Eiben B, Vavourakis V, Hipwell JH, Kabus S, Lorenz C, Buelow T, Hawkes DJ (2014) Breast deformation modelling: comparison of methods to obtain a patient specific unloaded configuration, vol 9036, pp 903615–8
11. Conley RH, Meszoely IM, Weis JA, Pheiffer TS, Arlinghaus LR, Yankeelov TE, Miga MI (2015) Realization of a biomechanical model-assisted image guidance system for breast cancer surgery using supine mri. Int J Comput Assist Radiol Surg 10(12):1985–1996
12. Lee A, Schnabel J, Rajagopal V, Nielsen P, Nash M (2010) Breast image registration by combining finite elements and free-form deformations. In: Digital mammography, pp 736–743
13. Carter T, Tanner C, Beechey-Newman N, Barratt D, Hawkes D (2008) Mr navigated breast surgery: method and initial clinical experience. In: Medical image computing and computer-assisted intervention–MICCAI, vol 2008, pp 356–363
14. Han L, Hipwell J, Mertzanidou T, Carter T, Modat M, Ourselin S, Hawkes D (2011) A hybrid fem-based method for aligning prone and supine images for image guided breast surgery. In: 2011 IEEE international symposium on biomedical imaging: from Nano to Macro. IEEE, pp 1239–1242
15. Pathmanathan P, Gavaghan DJ, Whiteley JP, Chapman SJ, Brady JM (2008) Predicting tumor location by modeling the deformation of the breast. IEEE Trans Biomed Eng 55(10):2471–2480
16. Patete P, Iacono MI, Spadea MF, Trecate G, Vergnaghi D, Mainardi LT, Baroni G (2013) A multi-tissue mass-spring model for computer assisted breast surgery. Med Eng Phys 35(1):47–53
17. Zerbato D, Baschirotto D, Baschirotto D, Botturi D, Fiorini P (2011) Gpu-based physical cut in interactive haptic simulations. Int J Comput Assist Radiol Surg 6(2):265–272
18. Pinto Pereira SM, Hipwell JH, McCormack VA, Tanner C, Moss SM, Wilkinson LS, Khoo LAL, Pagliari C, Skippage PL, Kliger CJ (2010) Automated registration of diagnostic to prediagnostic x-ray mammograms: evaluation and comparison to radiologists' accuracy. Med Phys 37(9):4530–4539
19. van Engeland S, Snoeren P, Hendriks JHCL, Karssemeijer N (2003) A comparison of methods for mammogram registration. IEEE Trans Med Imaging 22(11):1436–1444
20. Lautrup B (2011) Physics of continuous matter, 2nd edn: exotic and everyday phenomena in the macroscopic world. CRC Press, Boca Raton
21. Maas SA, Ellis BJ, Ateshian GA, Weiss JA (2012) Febio: finite elements for biomechanics. J Biomech Eng 134(1):011005
22. Besl PJ, McKay ND (1992) A method for registration of 3-d shapes. IEEE Trans Pattern Anal Mach Intell 14(2):239–256
23. Rankin A, Pinter C, Ungi T, Lasso A, Heffter T, Fichtinger G (2014) Plus: open-source toolkit for ultrasound-guided intervention systems. In: IEEE transactions on biomedical engineering
24. Zerbato D, Forgione A, Fiorini P (2016) University of Verona Santorzo Vicenza D. Dall'Alba, F. Bovo. Towards an intraoperative calibration-preserving freehand ultrasound system. In: Computer Assisted Radiology and Surgery (CARS)

Francesco Visentin received his Ph.D. and his Master's Degree from the University of Verona (Italy) respectively in 2017 and 2009. Since 2009, he is a member of the ALTAIR Robotic Laboratory (Verona, Italy), where he was involved as Research Fellow in different European founded projects. From 2013 to 2017, he was a visiting researcher at the Artificial Intelligence Laboratory, University of Tsukuba (Tsukuba, Japan). He is currently a Postdoc Researcher at the Center for Micro-BioRobotics of Istituto Italiano di Tecnologia, Pontedera, Italy. His research interests include Soft Deformable Robotics, Sensing and Sensor development, Biologically Inspired Robots, and Human-Robot Interaction.

Vincent Groenhuis received his B.Sc. with honors in Computer Science in 2006, and his MSc degree with honors in Embedded Systems in 2014, both at the University of Twente. He is currently pursuing a Ph.D. degree at the Department of Robotics and Mechatronics, University of Twente, Enschede, The Netherlands.

Bogdan Maris received a degree in Mathematics from the 'Babes-Bolyai' University, Cluj-Napoca, Romania, the Laurea in Computer Science, and the Ph.D degree in Computer Science from the University of Verona, Italy. Since 2008, he has been a Research Fellow with the ALTAIR Robotics Laboratory, Department of Computer Science, University of Verona, Italy. His research interest include medical image registration, minimally invasive surgical procedures, computer vision, robotics.

Diego Dall'Alba (male) received the Master Degree with honors in "Intelligent and multimedia systems" from the University of Verona, Italy, in 2010. He received Ph.D. in Computer Science from the University of Verona in 2014. Since 2008, he is a member of the Altair robotics laboratory (Verona, Italy) and he has been involved in 4 European projects: AccuRobAs, Safros, ISUR and MURAB. In 2012, he was visiting researcher at the University of British Columbia (Vancouver, Canada). He is currently working as Postdoc researcher and his main research interests are in the field of surgical robotics (advance sensing and multi-modal data processing), computer-assisted surgery, and ultrasound-guided system.

Françoise Siepel received her MSc in Technical Medicine from the University of Twente with specialty in Robotics and Imaging in 2010. After completion of her PhD in 3 years at the Stavanger University Hospital in Norway affiliated with the University of Bergen and competence as Technical physician, she is currently working as a postdoc in the Robotics and Mechatronics group, Faculty of Electrical Engineering, Mathematics & Computer Science, University of Twente.

Stefano Stramigioli received the MSc with honors (cum laude) in 1992 and the Ph.D with honors (cum laude) in 1998. He is currently full professor of Advanced Robotics and chair holder of the Robotics and Mechatronics group at the University of Twente. He has more than 200 publications including four books. He is currently the Vice President for Research of euRobotics, the private part of the PPP with the EU known as SPARC. He has been an Officer and AdCom member for IEEE RAS. He is an IEEE Fellow.

Paolo Fiorini (F'09) received the Laurea degree in electronic engineering from the University of Padua, Padua, Italy, the M.S.E.E. degree from the University of California at Irvine, Irvine, CA, USA, and the Ph.D. degree in mechanical engineering from the University of California at Los Angeles, Los Angeles, CA, USA. He was with the NASA Jet Propulsion Laboratory, California Institute of Technology, Pasadena, CA, USA, from 1985 to 2000, where he was involved in telerobotic and teleoperated systems for space exploration. From 2000 to 2009, he was an Associate Professor of Control Systems with the School of Science, University of Verona, Verona, Italy, where he founded the Altair Robotics Laboratory with his students. He is currently a Full Professor of Computer Science at the University of Verona. His current research interests include teleoperation for surgery, service, and exploration robotics funded by several European Projects.